Catalysis Science & Technology

Accepted Manuscript

ROYAL SOCIETY OF CHEMISTRY

www.rsc.org/catalysis

Catalytic properties of copper manganese mixed oxides prepared by coprecipitation using tetraammonium hydroxide

Running title: Catalytic properties of Cu-Mn mixed oxides

Hisahiro Einaga,*[a] Akihiro Kiya,[a] Satoru Yoshioka,[b] and Yasutake Teraoka[a]

[a]*Department of Energy and Material Sciences, Faculty of Engineering Sciences, Kyushu University, Kasuga, Fukuoka 816-8580, Japan.*

[b]*Department of Applied Quantum Physics and Nuclear Engineering, Faculty of Engineering, Kyushu University, 744, Motooka, Nishi-ku, Fukuoka 819-0395, Japan.*

**Corresponding author, phone: +81-92-583-7525; Fax: +81-92-583-8853.*

E-mail: einaga.hisahiro.399@m.kyushu-u.ac.jp

Copper-manganese (Cu-Mn) mixed oxide catalysts were prepared by coprecipitation technique from metal nitrates in aqueous solution using tetramethylammonium hydroxide (TMAH) as a pH regulator. The structures and properties of the mixed oxide catalysts were investigated by X-ray diffraction, extended X-ray absorption fine structure, X-ray photoelectron spectroscopy and H_2-TPR studies. Spinel type mixed oxides were mainly formed in the Cu-Mn mixed oxides, in which Cu and Mn species occupied both tetrahedrally and octahedrally coordinated sites. The occupancy of the Cu and Mn in the sites depended on the Cu/Mn ratio. The average oxidation state of Cu was evaluated to be 2+ and was almost independent of the Cu/Mn ratio, whereas reduced Cu species was also formed on the surface sites. By incorporation of Cu into Mn oxides, the average oxidation state of Mn increased both in the bulk sites and on the surface sites. The concentration of Mn on the surface sites was higher than that in the bulk sites. The Cu-Mn mixed catalysts exhibited higher activity than corresponding single metal oxides at the reaction temperature of 343-403 K. Formation of Cu-Mn spinel type oxides gave rise to the increase in the catalyst surface area and the rate for CO oxidation normalized by surface area, and the Cu-Mn mixed oxides with the Cu/Mn molar ratio of 1 exhibited the highest activity for CO oxidation. CO-TPR studies revealed that in the temperature range of 343-403 K, the lattice oxygen at the first layer of the mixed oxides reacted with CO to form CO_2.

Introduction

Catalytic oxidation of CO has been one of the important topics in the research area of catalysis science and is still an important technology for environmental protection. Noble metals, metal oxides and mixed metal oxides have been used for the reaction and the optimal catalyst composition for CO oxidation is different depending on the reaction conditions. At relatively low temperature (< 473 K), noble metal catalysts, platinum and palladium catalysts supported on high surface area carriers are effective for the reaction.[1,2] At room temperature, gold catalysts supported on TiO_2 and Fe_3O_4 exhibited high activity.[3-5] On the other hand, in the high temperature range (> 773 K), transition metal oxides and mixed metal oxides are preferable[6,7] because noble metal catalysts suffer from catalyst sintering, which generally gives rise to catalytic deactivation.

Copper-manganese (Cu-Mn) mixed oxides are also promising catalysts in oxidation processes at various reaction temperatures. As the conventional catalysts, hopcalite catalysts[8,9] with amorphous structures have been used for respiratory protection because they exhibit high CO oxidation activity even at room temperature.[10-13] At higher temperature, Cu-Mn mixed oxides with spinel phases have been reported to exhibit high activity for oxidation of CO[14] and organic compounds[15]. From the standpoint of industrial application, CO oxidation catalysts which consist of inexpensive transition metals and operate in the temperature range of 333-423 K are important. Under such conditions, Cu-Mn-O mixed oxides are good candidates for substitutes for noble metal catalysts.

Cu-Mn mixed oxides are generally prepared by coprecipitation[16,17], formate decomposition[18], redox[19,20], solid state reaction[21], and sol-gel methods[22]. As the most frequently used method, metal salts are hydrolyzed by alkaline salts, Na_2CO_3 or $NaHCO_3$ and the resulting Cu-Mn hydroxide precursors are calcined at 673 K. In this method, however, Na^+ remains in the mixed oxide catalysts as an impurity when after treatment process, namely washing process is insufficient.[23] The remaining Na^+ species has been reported to bring detrimental effects on their catalytic activity of the Cu-Mn mixed oxides for CO

oxidation.[24] Therefore, Na-free methods are promising for the preparation of Cu-Mn mixed oxides with high catalytic activities.

In this paper, we report on the method for preparation of Cu-Mn-O spinel-type oxides without use of Na-containing reagents. This method involves the hydrolysis of Cu and Mn nitrates in aqueous solution using tetramethylammonium hydroxide (TMAH) as a pH regulator. The resulting precipitates are calcined at 673 K. In this method, the dissolution of Cu^{2+} species in mother solution can be avoided, in marked contrast with the hydrolysis process using NH_3 where $[Cu(NH_3)_4]^{2+}$ complexes are formed in the preparation of Cu oxides. The method can prevent Na impurity remaining in the final products. The structure of the Cu-Mn mixed oxides and their catalytic properties for CO oxidation were investigated in detail.

Experimental

Catalyst preparation

All the chemicals used in this study were of analytical grade and used without further purification. Cu-Mn oxides were prepared by hydrolysis of metal nitrates in aqueous solutions. In a typical procedure, appropriate amounts of $Cu(NO_3)_2 \cdot 3H_2O$ (Wako Pure Chemical, Japan, >99.9%) and $Mn(NO_3)_2 \cdot 6H_2O$ (Wako Pure Chemical, Japan, >99.9%) were dissolved into water, and the aqueous solution was added dropwise to an aqueous solution which contained tetramethylammonium hydroxide (TMAH, Kishida Chemical Co., Ltd.). The resultant colloidal particles were filtered off and washed several time with water, followed by drying at 373 K for 24 h and calcination at 673 K for 5 h. In this method, Cu and Mn ions in the synthetic solutions were completely precipitated by the hydrolysis with TMAH and therefore the bulk molar ratio of Cu to Mn was consistent with that of the metal nitrate precursors used in the preparation procedures. The molar ratio of Cu to Mn in the final products was variously changed by changing the Cu/Mn ratio in the starting materials. For comparison, Cu and Mn single oxides were prepared under the same conditions. Hereafter, the Cu-Mn mixed oxides with the Cu/Mn molar ratio of 1/2, 1/1, and 2/1 were denoted by Cu-Mn(1-2), Cu-Mn(1-1), and Cu-Mn(2-1), respectively.

Catalyst characterization

X-ray diffraction (XRD) patterns were taken using a RIGAKU RINT2200 diffractometer using Cu Kα radiation. Catalyst surface area was determined by BET method from N_2 adsorption isotherm at 77K with Belsorp mini (BEL Japan Co. Ltd.). EXAFS and XANES spectra were taken at Kyushu University beamline in the Kyushu Synchrotron Light Research Center (SAGA-LS/BL-06) with the storage ring operating at an energy of 1.4 GeV. Catalyst samples were mixed with boron nitride (BN) and pressed into thin disks (20 mmϕ). EXAFS spectra were recorded at room temperature. Data reduction of experimental absorption spectra was carried out according to the method recommended by the Standards and Criteria Committee of the International XAFS Society[25] using a REX2000 software. EXAFS oscillations, χ(k),were extracted from the data using a smoothing spline and normalized to the edge height. Then, k^3-weighted EXAFS data ($k^3\chi(k)$) were Fourier transformed to R-space over 3.0-15.8 $Å^{-1}$ for Mn K edge and 2.3-14.0 $Å^{-1}$ for Cu K edge spectra. The inverse Fourier transformation to k-space was employed over for Mn K edge and Cu K edge spectra. EXAFS curve fitting was carried out for the spectra to obtain the coordination numbers (CN), bond distances (R), Debye-Waller factor (σ^2), and energy shift (ΔE) using theoretical backscattering amplitude and phase shift functions calculated by the program FEFF8.[26] For the curve-fitting, a maximum number of free parameters did not exceed the number n, which was estimated according to the Nyquist theoem[27]: $n = (2\Delta k\Delta r/p) + 1$, where Δk and Δr, are the k (where k is the wave vector) and r (where r is the distance from the absorber atom) ranges, respectively. The validity of the theoretical parameters was checked by running the reference samples (MnO, Mn_3O_4, Mn_2O_3 and MnO_2 for Mn K edge and Cu, Cu_2O, and CuO for Cu K edge spectra).

XANES spectra were obtained after background-corrected and normalized spectra were transformed to the first derivatives. The absorption edge was estimated from the inflection points of the spectra.

XPS spectra were recorded with a Kratos ESCA-3400 spectrometer with a Mg Kα source (1253.6 eV). The binding energies were corrected using the values of 284.8 eV for the C 1s peak of the carbon species on the catalyst samples as an internal standard. XPS intensity ratios were determined using the integrated

areas of the Cu $2p_{3/2}$ and Mn $2p_{3/2}$ photoelectron lines. The surface atomic ratios of Cu/Mn were calculated from equation (1).

$$\frac{I_{Mn}}{I_{Cu}} = \frac{\sigma_{Mn}\lambda_{Mn}d_{Mn}}{\sigma_{Cu}\lambda_{Cu}d_{Cu}} \quad (1)$$

Here, I_{Cu} and I_{Mn} are the integrated peak intensities of Cu $2p_{3/2}$ and Mn $2p_{3/2}$, respectively. σ_{Cu} and σ_{Mn} are the Scofield photoelectron cross sections for Cu $2p_{3/2}$ and Mn $2p_{3/2}$ respectively. λ_{Cu} and λ_{Mn} are the inelastic mean free paths of Cu $2p_{3/2}$ and Mn $2p_{3/2}$, respectively. d_{Cu} and d_{Mn} are the numbers of Cu and Mn atoms in unit volumes, respectively.

Temperature-programmed reduction with H_2 (H_2-TPR) was performed using the flow-type BELCAT-30 catalyst analyzer (BEL JAPAN, Inc). The sample (0.050 g) was pretreated in an O_2 flow for 2 h at 773 K. In the H_2-TPR measurements, catalyst samples were heated at the rate of 10 K/min.

Catalytic CO oxidation

Catalytic oxidation of CO was carried out with a fixed bed flow reactor. The reaction gases for CO oxidation were prepared by mixing CO (1%, He balance), O_2 (0.5%, He balance; 10%, He balance) and He in cylinders (reaction gas: CO concentration 0.5%, O_2 10% or 0.25%; gas flow rate 100 ml min^{-1}; catalyst weight 0.050 g; WHSV = 120,000 mL g^{-1} h^{-1}). Prior to catalytic reaction, the catalyst was heated at 573 K in a flow of pure O_2 for 1 h, and then thermostated at a reaction temperature (343-423 K) with a heating apparatus. Gas samples were analyzed on a GC-TCD (Shimadzu GC-14B). In the case of temperature programmed reduction with CO, gas samples were analyzed by an FTIR spectrometer (Perkin-Elmer Spectrum One) equipped with a 2.4 m optical length gas cell (volume 100 mL).

Results and discussion

Structures of Cu-Mn mixed oxides

Fig. 1 shows the XRD patterns of the Cu-Mn mixed oxides prepared by hydrolysis of Cu and Mn nitrates with TMAH in aqueous solution and calcined at 673 K. The peaks for spinel phases were

observed for Cu-Mn(1-2), Cu-Mn(1-1), and Cu-Mn(2-1). The peaks due to CuO were also detected for Cu-Mn(1-1), and Cu-Mn(2-1), and their intensity increased with increasing the Cu/Mn ratio. For comparison, Cu and Mn single oxides prepared by the same method were also shown in Fig. 1. For the Cu single oxide (CuOx), all the peaks were indexed by the diffraction for CuO phases and no other peaks were detected. For the Mn single oxides (MnOx), the crystal phases of Mn_3O_4 and Mn_2O_3 were observed. Table 1 summarizes textural properties of the Cu-Mn mixed oxides. BET surface areas of the mixed oxides were larger than those of the single oxides: the largest surface area was obtained for Cu-Mn(1-1), and the surface area of Cu-Mn(1-1) was 2.5-7 times larger than that of CuOx and MnOx.

Fig. 2 shows the Mn-K edge EXAFS spectra of Cu-Mn mixed oxides and MnOx prepared by coprecipitation with TMAH and calcined at 673 K (Fig. 2(a)). For comparison, the spectra of references samples, MnO, Mn_3O_4, Mn_2O_3, and MnO_2 were also shown in Fig. 2(b). For the MnOx sample, the peak positions are very close to those of reference sample, Mn_3O_4: the peak due to Mn-O in the first coordination sphere was observed at 1.56 Å (phase uncorrected: pu), and the peaks due to Mn-Mn in the second coordination sphere at 2.52 (pu) and 2.95 (pu), which were mainly ascribed to Mn-Mn contributions. For the Cu-Mn mixed oxides, the peak positions were different from those of reference samples: strong peaks appeared at 1.56 (pu) and 2.52 Å (pu) along with the small peak at 3.10 Å (pu) for Cu-Mn(1-1). Thus, the local structures of the Mn in the mixed oxides were much different from those of MnOx. Theoretical simulation revealed that, in the case of Cu-Mn-O mixed oxides, the strong peak at 2.58 Å (pu) was mainly ascribed to the contributions of Mn-Cu and Mn-Mn bonds in Cu-Mn spinel phase. The peak position was almost the same for Cu-Mn(1-2) and Cu-Mn(2-1), whereas the peak intensities were slightly different depending on the Cu/Mn ratio.

The Cu-K edge EXAFS spectra of Cu-Mn oxides are shown in Fig. 3. For CuOx, the peaks were observed at 1.56, 2.52 and 2.98 Å (pu). According to the XRD studies described above, CuOx has the CuO structure in which two oxygen atoms are axially coordinated and four oxygen

atoms are equatorially coordinated to Cu. The axial Cu-O bond lengths are longer than the equatorial Cu-O bond lengths. Accordingly, the first coordination shell in the EXAFS spectrum was attributed to four equatorial oxygen atoms, and the second coordination shell at 2.98 Å (pu) was ascribed to Cu-Cu and Cu-O contributions. Upon the addition of Mn to Cu oxide, the peak positions at 2.64 and 3.07 Å (pu) were almost unchanged but the intensities were changed. For the Cu-Mn mixed oxides, the peak of Cu-O was observed at 1.56 Å (pu), whereas the peaks at 2.64 and 3.07 Å (pu) were attributable to Cu-Mn and Cu-Cu contributions in Cu-Mn spinel phases. In the case of Cu-Mn(1-1) and Cu-Mn(1-2), the Cu-Cu bonds in impurity CuO also contributed to the peaks at 2.64 and 3.07 Å (pu).

The ideal crystal structure of $(Cu_2)[Mn_3Cu]O_8$ is a spinel structure with a cubic lattice containing one type of Mn atom and two types of Cu atoms.[28] The Mn atoms are located in the octahedral sites which have six Mn-O bonds of the length in the range of 1.82-2.04 Å, two Mn-Cu bonds of the length 2.90 Å, four Mn-Mn bonds of 2.95 Å, and two Mn-Cu bonds of length 3.34 Å. The first type of Cu is located in the tetrahedral sites which have a four Cu-O bonds of length ca. 2.0 Å, three Cu-Mn bonds of 3.34 Å, and three Cu-Cu bonds of 3.38 Å. The second type of Cu is located in octahedral sites which have six Cu-O bonds of lengths of 2.08 Å, six Cu-Mn bonds of length 2.90 Å, and six Cu-Cu bonds of length 3.38 Å. On the basis of structural consideration described above, the quantitative analysis was performed on the Mn K edge EXAFS spectra and fitting data are summarized in Table 2. Here, the first coordination shell, namely the peak at 1.56 Å (pu) was fitted with a Mn-O single scattering path and the second coordination shell was fitted with Mn-Cu and Mn-Mn single scattering paths. No multiple scattering paths were considered. Under the condition, a maximum number of free parameters did not exceed the number n, which was estimated according to the Nyquist theorem.[27]

The fitting results listed in Table 2 indicate that the EXAFS spectra of the Cu-Mn mixed oxides were fitted well with the structural parameters of $Cu_3Mn_3O_8$ phase. When the Cu/Mn ratio was changed, no significant changes were observed for Mn-O length in the first coordination shell and

Mn-Cu and Mn-Mn lengths for the second coordination shell. The Mn-O coordination number was in the range of 4-6 and higher for Cu-Mn(2-1) than the coordination numbers for Cu-Mn(1-1) and Cu-Mn(1-2). The Mn-Cu coordination number for the bond length of ca 2.9 Å correlates with the occupancy of the Mn atoms in the octahedral sites. As the occupancy of Mn in the octahedral site increased and that in the tetrahedral site decreased, the Mn-Cu coordination numbers at 2.9 Å increased. These indicate that Mn atoms occupied the tetrahedral sites as well as the octahedral sites and that the occupancy of Mn atoms in the octahedral sites was the largest for Cu-Mn(2-1) among the mixed oxides.

The curve fitting results for Cu-K edge EXAFS spectra are listed in Table 3. For Cu-Mn(1-2), the peak at 1.56 Å (pu) was fitted with a Cu-O single scattering path and the peaks at 2.64 and 3.07 Å (pu) were fitted well with two Cu-Mn single scattering paths and a Cu-Cu single scattering path in the $Cu_3Mn_3O_8$ spinel phase. The comparison of the fitting results in Table 2 and 3 revealed that the Cu-Mn bond lengths determined from Mn K edge spectra were almost consistent with those obtained from the Cu K edge spectra. CuO phase was also present in Cu-Mn(1-1) and Cu-Mn(2-1), as evidenced from XRD studies. Therefore, the contribution of Cu-Cu bond in the CuO phase cannot be neglected and curve fitting including the CuO phase cannot be performed because the maximum number of free parameters exceeded the number n which was estimated according to the Nyquist theorem. It is worth to note that the Cu-K edge EXAFS spectra of Cu-Mn(1-2) cannot be fitted with Cu-O, Cu-Cu, and Cu-Mn bonds in ideal $CuMn_2O_4$ phase in which Cu was located only in the tetrahedral sites. This finding further indicates that Cu was located in both octahedral and tetrahedral sites of the Cu-Mn spinel phases.

The oxidation state of Cu and Mn

Fig. 4 shows the Mn-K edge XANES spectra of Cu-Mn mixed oxides (Fig. 4(a)). The absorption edge of the XANES spectra was reported to be correlated with the oxidation state of Mn of manganese oxides.[29-31] The absorption edge (E_0) was estimated from the inflection point of the

first derivatives of the XANES spectra, which shows the linear relationship between the oxidation state and E_0 value (Supplementary information). From the relationship, the average oxidation state of Mn in the Cu-Mn mixed oxides was determined and listed in Table 4. The average oxidation state for MnOx was 2.8, which was consistent with the results that Mn_2O_3 and Mn_3O_4 were observed in the XRD patterns. It is likely that Mn_3O_4 phase was the main component of MnOx. For the Cu-Mn mixed oxides, the average oxidation state of Mn increased to 3.2, indicating that the Mn species were oxidized by the addition of Cu. However, the average oxidation state was independent of the Cu/Mn ratio.

Fig. 5 shows the Cu-K edge XANES spectra of Cu-Mn mixed oxides and reference samples. Cu_2O and CuO were characterized by the peak positions for strong white line and absorption edge of the XANES spectra.[32-34] The white lines for Cu_2O and CuO were observed at 8992 and 8995 eV, respectively, and the absorption edge for CuO was higher in 5 eV than that for Cu_2O. In the first derivatives of the spectra, strong peaks were observed at 8985 and 8992 eV for CuO, whereas strong peaks positioned at 8982 and 8986 eV for Cu_2O. The peak positions for the Cu-Mn mixed oxides were very close to those for CuO, suggesting that Cu^{2+} species were mainly present in the mixed oxides and the average oxidation state of Cu was not almost affected by the Mn/Cu ratio.

The surface state of Cu-Mn oxides was investigated by X-ray photoelectron spectroscopic studies. Fig. 6 shows the XPS spectra of the Cu-Mn mixed oxides and single oxides in the range of 930-970 eV. As shown in Fig. 6(a), Cu $2p_{1/2}$ and Cu $2p_{3/2}$ peaks for Cu^{2+} species[35,36] with satellite peaks due to charge transfer were observed for Cu-Mn mixed oxides and CuOx, indicating that Cu^{2+} species were mainly present on the surface of these samples. For the mixed oxides, the peak due to Cu^+ (or Cu^0) species at 933.1 eV also appeared along with the Cu^{2+} peaks, and the peak intensity for the reduced Cu species relatively increased with increasing the Mn/Cu ratio.

XPS spectra also exhibited the spin-orbit splitting of Mn $2p_{1/2}$ and Mn $2p_{3/2}$ signals in the range of 635-660 eV. For MnOx, the peak position of Mn $2p_{3/2}$ signal was located in the range of 641.5±0.1 eV, indicating that the Mn species on the surface sites was mainly composed of

Mn^{3+}.[37,38] In the case of Cu-Mn(1-1) and Cu-Mn(1-2), the Mn $2p_{3/2}$ peak was located in the range of 641.5±0.1 eV, whereas FWHM (full width at half maximum) for the Mn $2p_{3/2}$ signal was larger than that for MnOx. In addition, the Mn $2p_{3/2}$ signal for Cu-Mn(2-1) was observed at 641.9 eV. These findings suggesting that Mn^{4+} ion was also formed in the Cu-Mn oxides, and the amount of Mn^{4+} ion increased with increasing the Cu/Mn ratio. The molar ratios of Mn/Cu for the surface site of the Cu-Mn mixed oxides were estimated from the XPS peak intensities and listed in Table 4. It is noteworthy that the molar ratios of Mn/Cu on the catalyst surface were much larger than those in the bulk sites.

H_2-TPR studies

Temperature programmed reduction profiles of Cu-Mn mixed oxides and single oxides with H_2 were shown in Fig. 7. MnOx exhibited the two reduction peaks in the temperature ranges of 500-600 K and 600-750 K. The first peak was ascribed to the reduction of Mn_2O_3 to Mn_3O_4, and the second to the reduction of Mn_3O_4 to MnO.[39] The reduction of CuO with H_2 proceeded in the temperature range of 400-610 K. On the other hand, in the case of Cu-Mn mixed oxides, the second reduction peak of Mn disappeared, indicating that the temperature for Mn reduction decreased by the presence of Cu in the catalysts. In this reduction process, Cu^{2+} species were at first reduced to Cu^0 and the copper site acts as the H_2 activation sites and the reduction of Mn oxides with H_2 was promoted. The promotion of Mn reduction by Cu indicated that the Cu and Mn species in the mixed oxides were located in close proximity.

On the basis of the TPR profiles, the amount of H_2 consumption was determined and the oxidation states of Cu and Mn were estimated. As described above, Cu species in the bulk sites was mainly Cu^{2+} and almost unchanged when the Cu/Mn composition was variously changed. Assuming that all the Cu species in the Cu-Mn mixed oxides have the oxidation state of 2+, the average oxidation state of Mn was determined and listed in Table 4. The value was almost consistent with the values obtained from the XANES studies. According to the amount of H_2

consumed in the H_2-TPR, the chemical composition of Cu-Mn(1-1) was determined to be $CuMnO_{2.65}$, which was very close to the chemical composition of $Cu_3Mn_3O_8$. The chemical composition of Cu-Mn(1-2), Cu-Mn(1-1), and Cu-Mn(2-1) was evaluated to be $CuMn_2O_{4.2}$, $CuMnO_{2.65}$, and $Cu_2MnO_{3.6}$, respectively. The chemical composition of Mn and Cu oxides was evaluated to be $MnO_{1.4}$ and $CuO_{1.0}$, respectively.

As described above, XRD, EXAFS, and H_2-TPR studies revealed that Cu-Mn spinel phases were mainly formed in the Cu-Mn mixed oxides. The XPS studies revealed that in the Cu-Mn mixed oxides and CuOx, chemical states of Cu and Mn on the surface sites were much different from those in the bulk sites. The average oxidation state of Cu in the bulk sites was mainly 2+ and not affected by the Cu/Mn ratio in the catalysts, whereas Cu species on the surface sites was partly reduced to 1+ by the addition of Mn to Cu oxides. It is likely that redox reaction between Cu and Mn species took place on their surface sites (eq.(2)), as reported in the previous studies.[40]

$$Cu(II) + Mn(III) \rightarrow Cu(I) + Mn(IV) \quad (2)$$

Thus, the average oxidation state of Mn species on the surface site was higher than that in the bulk sites. In addition, the concentration of Mn on the surface sites was higher than that in the bulk sites, as mentioned above. However, we also cannot exclude the possibility that formation of the reduced Cu species was ascribed to high vacuum condition during XPS measurement.

The H_2-TPR profiles also provided the information on the reducibility of Cu-Mn mixed oxides. The reduction of Cu-Mn(1-1) with H_2 started at around 333 K, and the temperature for catalyst reduction was lower than that for Cu and Mn single oxides. This indicates that the formation of Cu-Mn mixed oxide phases resulted in the enhanced reactivity of lattice oxygen.

Catalytic activities of Cu-Mn mixed oxides for CO oxidation

Fig. 8 shows the CO oxidation activities of Cu-Mn mixed oxides at various temperatures (343-403 K). MnOx exhibited almost no activities in this temperature range. The dependency of the activity on reaction temperature was much different depending on the chemical compositions.

The activity of CuOx for CO oxidation was quite low at the temperature lower than 373 K, but steeply increased in the higher temperature range. The CO oxidation activity with Cu-Mn mixed oxides was higher than that with Cu and Mn single oxides at lower temperature (< 373 K), and the highest activity was obtained with Cu-Mn(1-1). The CO oxidation activity with Cu-Mn(1-1) and Cu(1-2) monotonously increased with the increase in reaction temperature. On the other hand, the increment of CO oxidation activity was much larger for Cu-Mn(2-1) than Cu-Mn(1-1) and Cu-Mn(1-2) at the temperature higher than 373 K. It is likely that the impurity CuO in Cu-Mn(2-1) contributed to CO oxidation at high temperatures (> 373 K).

The rate for CO oxidation normalized by surface area with Cu-Mn mixed oxides is listed in Table 5. The rate was evaluated at 358 K, where the CuO phase hardly contributed to CO oxidation and the CO oxidation almost proceeded on Cu-Mn mixed oxide phases. The rate decreased in the order: Cu-Mn(2-1) > Cu-Mn(1-1) > CuO ~ Cu-Mn(1-2) > MnOx. Thus, the CO oxidation rate normalized by surface area was also improved by the formation of Cu-Mn mixed oxides. The higher activity of Cu-Mn(1-1) than single oxides was ascribed to the improvement in catalyst surface area and higher activity per catalyst surface area. Cu-Mn(2-1) exhibited the highest activity among the Cu-Mn mixed oxides and single oxides for CO oxidation when the activities were normalized by catalyst surface area, whereas its surface area was much lower than Cu-Mn(1-1). Although Cu-Mn(1-2) has larger surface area than Cu and Mn single oxides, the rate normalized by surface area for Cu-Mn(1-2) was much lower than the rates for Cu-Mn(1-1) and Cu-Mn(2-1).

It has been reported that CO oxidation on Cu-Mn mixed oxides proceeds by Langmuir-Hinshelwood mechanism in which CO and O_2 are coadsorbed on the catalyst surface, followed by surface reaction between the adsorbed species[40] or Mars-van-Krevelen mechanism in which lattice oxygen takes part in the CO oxidation, followed by catalyst reoxidation[41]. The reaction pathways depended on the catalyst properties and reaction conditions. As described above, the reactivity of the lattice oxygen was the highest for Cu-Mn(1-1) among the catalysts

tested in this study. One of the possible explanations for the higher activity of Cu-Mn(1-1) than single oxides was its high reducibility, namely the reactivity of lattice oxygen.

The consideration described above urged us to investigate the reactivity of oxygen species of Cu-Mn mixed oxides for CO oxidation. Fig. 9 shows the temperature programmed reduction of Cu-Mn(1-1) with CO (CO-TPR) (Fig.9(a)). Here, the catalyst was heated from room temperature to 773 K with the rate of 10 K/min in a N_2 flow. Under the O_2-absent conditions, lattice oxygen or adsorbed O_2 species on the catalyst reacted with CO to give CO_2. The amount of CO_2 formed increased with the increase in reaction temperature. In this process, the amount of CO reacted was consistent with that of CO_2 formed. The CO-TPR profile showed a plateau at the temperature of 402 K, where the amount of CO reacted was estimated to be 1.72×10^{-4} mol/g-catalyst, which corresponded to 1.04% of total lattice oxygen of Cu-Mn(1-1). The value corresponded to two oxygen atoms per 1 nm^2 of catalyst surface area, which was lower than the amount of lattice oxygen at the first layer of surface (1.13×10^{-3} mol/g-catalyst), assuming the (100) planes of $Cu_3Mn_3O_8$ structures. Therefore, it is plausible that surface lattice oxygen and/or adsorbed oxygen on the surface reacted with CO at the temperature lower than 402 K. Up to the second plateau at 583 K, the amount of CO_2 converted was 1.62×10^{-3} mol/g-catalyst, which corresponded to 9.76% of total lattice oxygen of Cu-Mn(1-1). At this stage, oxygen atoms at surface 1.5 layers were reacted with CO, indicating that the lattice oxygen predominantly contributed to the CO oxidation.

Fig. 9 also compared the CO-TPR profiles for the Cu-Mn(1-2) and Cu-Mn(2-1) catalysts (Fig. 9(b) and (c)). CO oxidation to CO_2 proceeded and the profiles were much different from those for Cu-Mn(1-1). The total amount of oxygen reacted with CO in the profiles was estimated to be 4.47×10^{-3} and 3.75×10^{-3} mol/g-catalyst for the Cu-Mn(1-2) and Cu-Mn(2-1) catalysts, which corresponded to 25.6% and 25.0% of total lattice oxygen of the catalysts, respectively. This indicates that the lattice oxygen of the Cu-Mn(1-2) and Cu-Mn(2-1) catalysts are reacted with CO. Below the temperature of 403 K, the amount of oxygen reacted with CO was in the order:

Cu-Mn(1-1)>Cu-Mn(2-1)>Cu-Mn(1-2), which correspond to the order of catalytic properties for CO oxidation.

The finding described above implies that the reactivity of oxygen species is affected by the chemical composition. For the Cu-Mn(1-1) and Cu(2-1) catalysts, which exhibited high CO oxidation rate normalized by surface area, the Mn/Cu ratio on the catalyst surface was 1.6 and 0.9, respectively. On the other hand, the Mn/Cu ratio for Cu-Mn(1-2) was much low compared with Cu-Mn(1-1) and Cu(2-1) catalysts. Therefore, the formation of the Cu-O-Mn linkages, which is likely to be the key active sites, was higher for Cu-Mn(1-1) and Cu(2-1) catalysts than Cu-Mn(1-2). Thus, the optimization of the surface composition is crucial to obtaining high catalytic activities for CO oxidation. In addition, the changes of the oxidation state of Cu and Mn species can affect the catalytic properties of Cu-Mn mixed oxides.[40]

Conclusions

In this study, we reported a simple method for preparation of Cu-Mn spinel oxides. The method used tetramethylammonium hydroxide (TMAH) as a pH controlling agents for coprecipitation of Cu and Mn nitrates in the aqueous solution. The resulting precipitates were dried and calcined at 673 K. XRD and EXAFS studies showed that spinel type Cu-Mn mixed oxides were formed. The Cu and Mn species were located in both tetrahedral sites and octahedral sites, and the occupancy depended on the Cu/Mn ratio. Cu^{2+}, Mn^{3+}, and Mn^{4+} species were formed in the Cu-Mn mixed oxides in the mixed oxides. The reducibility of Cu-Mn mixed oxides was improved by the formation of mixed oxides. The surface area was much increased by the formation of mixed oxides and the highest activity was obtained at the Cu/Mn ratio of 1. The highest activity of Cu-Mn mixed oxides with the Cu/Mn ratio of 1 was obtained because the catalysts has the largest surface area and the highest activity when it was normalized by surface area. The oxygen species at the first layer of Cu-Mn mixed oxides participates in the CO oxidation, and thus the activity was strongly affected by the surface state: the formation of Cu-O-Mn linkages is crucial to

obtaining the high catalytic activities. The results described suggest that the precipitation method using TMAH is promising for preparation of Cu-Mn mixed oxides for catalytic CO oxidation.

Acknowledgements

This study was financially supported by New Energy and Industrial Technology Development Organization.

References

1 G. S. Zafiris, and R. J. Gorte, *J. Catal.,* 1993, **140,** 418.

2 S. Ladas, and H. Poppa, M. Boudart, *Surf Sci.,* 1981, **102,** l51.

3 M. Haruta, N. Yamada, T. Kobayashi, and S. Iijima, *J. Catal.,* 1989, **115,** 301.

4 M. Daté, M. Okumura, S. Tsubota, and M. Haruta, *Angew. Chem. Int. Ed.,* 2004, **43,** 2129.

5 M. Haruta, S. Tsubota, T. Kobayashi, H. Kageyama, M. J. Genet, and B. Delmon, *J. Catal.,* 1993, **144,** 175.

6 S. Royer, and D. Duprez, ChemCatChem, 2011, **3,** 24.

7 H. Falcón, M. J. Martinez-Lope, J. A. Alonso, and J.L.G. Fierro, *Appl. Catal. B: Environ.,* 2000, **26,** 131.

8 T. H. Rogers, C. S. Piggot, W. H. Bahlke, and J. M. Jennings, *J. Am. Chem. Soc.,* 1921, **43,** 1973.

9 S. Veprek, D. L. Cocke, S. Kehl, and H. R. Oswald, *J. Catal.,* 1986, **100,** 250.

10 L.-N. Cai, Y. Guo, A.-H. Lu, P. Branton, and W. C. Li, *J. Mol. Catal. A: Chem.,* 2012, **360,** 35.

11 C. Jones, K. J. Cole, S. H. Taylor, M. J. Crudace, and G. J. Hutchings, *J. Mol. Catal. A: Chem.,* 2009, **305,** 121.

12 G. J. Hutchings, A. A. Mirzaei, R. W. Joyner, M. R. H. Siddiqui, and S. H. Taylor, *Appl. Catal. A: Gen.,* 1998, **166,** 143.

13 S. A. Kondrat, T. E. Davies, Z. Zu, P. Boldrin, J. K. Bartley, A. F. Carley, S. H. Taylor, M. J. Rosseinsky, and G. J. Hutchings, *J. Catal.,* 2011, **281,** 279.

14 G. Fortunato, H. R. Oswald, and A. Reller, *J. Mater. Chem.,* 2001, **11,** 905.

15 S. A. Hosseini, A. Niaei, D. Salari, M.C. Alvarez-Galvan, and J. L. G. Fierro, Ceram. Int., 2014, **40,** 6157.

16 P. A. Wright, S. Natarajan, J. M. Thomas, and P. L. Gai-Boyes, *Chem. Mater.,* 1992, **4,** 1053.

17 P. Porta, G. Moretti, M. Musicanti and A. Nardella, *Solid State Ion.,* 1993, **63-65,** 257.

18 V. Koleva, D. Stoilova, and D. Mehandjiev, *J. Solid State Chem.,* 1997, **133,** 416.

19 E. C. Njagi, C.-H. Chen, H. Genuino, H. Galindo, H. Huang, and S. L. Suib, *Appl. Catal. B: Environ.,* 2010, **99,** 103.

20 E. C. Njagi, H. C. Genuino, C. K. King'ondu, C.-H. Chen, D. Horvath, and S. L. Suib, *Int. J. Hydro. Energy,* 2011, **36,** 6768.

21 D. P. Shoemaker, J. Li, and R. Seshadri, *J. Am. Chem. Soc.,* 2009, **131,** 11450.

22 M. Krämer, T. Schmidt, K. Stöwe, and W.F. Maier, *Appl. Catal. A: Gen.*, 2006, **302,** 257

23 H. Einaga, M. Maeda, and Y. Teraoka, *Appl. Catal. B: Environ.,* 2013, **142-143,** 406.

24 A. A. Mirzaei, H. R. Shaterian, R. W. Joyner, M. Stockenhuber, S. H. Taylor, and G. J. Hutchings, *Catal. Communi.,* 2003, **4,** 17.

25 D.C. Koningsberger, *Jpn. J. Appl. Phys., Suppl.*1993, **32-2,** 877.

26 A. L. Ankudinov, B. Ravel, J. J. Rehr, and S. D. Conradson, *Phys. Rev.,* 1998, **58,** 7565.

27 E.A. Stern, *Phys. Rev. B,* 1993, **48,** 9825.

28 R. E. Vandenberghe, E. Legrand, D. Scheerlinck and V. A. M. Brabers, *Acta. Cryst., B,* 1976, **32,** 2796.

29 T. Ressler, S. L. Brock, J. Wong, and S. L. Suib, *J. Phys. Chem. B,* 1999, **103,** 6407.

30 T. Ressler, J. Wong, J. Roots, and I.L. Smith, *Environ. Sci. Technol.,* 2000, **34,** 950.

31 J.M. Ramallo-López, E.J. Lede, F.G. Requejo, J.A. Rodriguez, J.-Y. Kim, R. Rosas-Salas, and J.M. Domínguezm, *J. Phys. Chem. B,* 2004, **108,** 20005.

32 C. Lamberti, S. Bordiga, F. Bonino, C. Prestipino, G. Berlier, L. Capello, F. D'Acapito, F. X. L. I. Xamena, and A. Zecchina, *Phys. Chem. Chem. Phys.,* 2003, **5,** 4502.

33 C. Prestipino, G. Berlier, F. X. L. I. Xamena, G. Spoto, S. Bordiga, A. Zecchina, G. T. Palomino, T. Yamamoto, and C. Lamberti, *Chem. Phys. Lett.,* 2002, **363,** 389.

34 A. Al-Ebraheem, J. Goettlicher, K. Geraki, S. Ralph, and M. J. Farquharson, *X-Ray Spectrom.,* 2010, **39,** 332.

35 N. Pauly, S. Tougaard, and F. Yubero, *Surf. Sci.,* 2014, **620,** 17.

36 J. Ghijsen, L.H. Tjeng, J. van Elp, H. Eskes, J. Westerink, and G.A. Sawatzky, *Phys. Rev. B,* 1988, **38,** 11322.

37 B.R. Strohmeier, and D.M. Hercules, *J. Phys. Chem.,* 1984, **88,** 4922.

38 A. A. Mirzaei, H. R. Shaterian, and M. Kaykhaii, *Appl. Surf. Sci.,* 2005, **239,** 246.

39 F. Kapteijn, A.S. Vanlangeveld, J.A. Moulijn, A. Andreini, M.A. Vuurman, A.M. Turek, J.M. Jehng, and I.E. Wachs, *J. Catal.,* 1994, **150,** 94.

40 S. Veprek, D. L. Cocke, S. Kehl, and H. R. Oswald, *J. Catal.,* 1986, **100,** 250.

41 K. Morgan, K. J. Cole, A. Goguet, C. Hardacre, G. J. Hutchings, N. Maguire, S. O. Shekhtman, S. H. Taylor, *J. Catal.,* 2010, **276,** 38.

Table 1 Textural properties of the Cu-Mn mixed oxides

Catalyst	The average oxidation state of Mn		BET surface area
	XANES	H_2-TPR	/ m^2 g^{-1}
CuOx	—	—	8.4
Cu-Mn (2-1)	3.2	3.2	10.5
Cu-Mn (1-1)	3.2	3.2	58.0
Cu-Mn (1-2)	3.2	3.2	40.4
MnOx	2.7	2.8	21.9

Table 2 Mn-K edge EXAFS curve-fitting results for Cu-Mn mixed oxide catalysts

Catalyst	Shell	CN	R / Å	σ^2 / 10^{-5} nm^2	ΔE / eV	R_f / % [a]
Cu-Mn(1-2)	Mn-O	4.7±0.2	1.927±0.01	6.40	-1.09	
	Mn-Cu	1.1±0.3	2.898±0.03	6.24	-1.18	2.5
	Mn-Mn	2.3±0.6	2.936±0.03	6.24	-1.55	
Cu-Mn(1-1)	Mn-O	4.6±0.2	1.929±0.01	6.40	-1.63	
	Mn-Cu	1.1±0.2	2.900±0.03	5.63	-2.45	1.8
	Mn-Mn	2.3±0.5	2.936±0.03	6.72	-2.12	
Cu-Mn(2-1)	Mn-O	5.4±0.2	1.924±0.01	6.24	-1.63	
	Mn-Cu	1.6±0.3	2.902±0.03	6.08	-2.12	2.4
	Mn-Mn	3.3±0.6	2.936±0.03	6.24	-3.36	
MnOx	Mn-O	5.8±0.2	1.934±0.01	4.36	-5.41	
	Mn-Mn	1.2±0.1	2.865±0.03	3.60	-6.32	2.1
	Mn-Mn	2.0±0.2	3.172±0.03	4.36	2.96	

[a]The residual factor: $R_f(\%) = \frac{\sum \{k^3\chi(k)_{obs} - k^3\chi(k)_{calc}\}^2}{\sum \{k^3\chi(k)_{obs}\}^2} \times 100$

Table 3 Cu-K edge EXAFS curve-fitting results for Cu-Mn mixed oxide catalysts

Catalyst	Shell	CN	R / Å	σ^2 / 10^{-5} nm^2	ΔE / eV	R_f / % [a]
Cu-Mn(1-2)	Cu-O	4.2±0.2	1.961±0.01	5.48	-6.57	2.7
	Cu-Mn	2.0±0.3	2.908±0.03	6.72	-7.85	
	Cu-Cu	4.8±0.6	3.345±0.03	6.89	-8.75	
	Cu-Mn	5.2±1.0	3.480±0.03	6.56	-5.31	
CuOx	Cu-O	3.8±0.2	1.944±0.01	3.72	-2.77	1.6
	Cu-O	1.7±0.3	2.716±0.03	3.72	-7.87	
	Cu-Cu	4.4±0.9	2.871±0.03	4.36	-8.35	
	Cu-Cu	1.5±0.9	3.375±0.03	4.62	-11.93	

[a]The residual factor: $R_f(\%) = \frac{\sum \{k^3\chi(k)_{obs} - k^3\chi(k)_{calc}\}^2}{\sum \{k^3\chi(k)_{obs}\}^2} \times 100$

Table 4 XPS analysis for Mn 2p peaks Cu-Mn mixed oxides

Catalyst	$Mn2p_{3/2}$	$Mn2p_{1/2}$	FWHM for $Mn2p_{3/2}$	O1s	Mn/Cu mole ratio
CuOx	—	—	—	531.4	—
Cu-Mn (2-1)	641.9	653.8	4.5	529.5	0.9
Cu-Mn (1-1)	641.5	653.4	4.2	529.3	1.6
Cu-Mn (1-2)	641.6	653.5	4.4	529.3	5.6
MnOx	641.6	653.6	3.7	532.1	—

Table 5 CO oxidation activities with Cu-Mn mixed oxides.

Catalyst	Rate per catalyst weight /$\times 10^{-5}$ mol min^{-1} g^{-1}	Rate per catalyst surface area /$\times 10^{-6}$ mol min^{-1} m^{-2}
CuOx	0.32	0.38
Cu-Mn 2-1	0.44	2.08
Cu-Mn 1-1	5.86	1.01
Cu-Mn 1-2	1.26	0.31
MnOx	0.06	0.03

Catalyst weight: 0.10 g; CO 0.5%-O_2 5%-He balance; gas flow rate: 100 mL/min (WHSV = 60,000 mL g-1 h-1); reaction temperature 358 K.

Figure captions

Fig. 1 XRD patterns of Cu-Mn mixed oxides.

Fig. 2 Mn-K edge EXAFS spectra of Cu-Mn mixed oxides. (a) Cu-Mn mixed oxides, (b) Mn single oxides.

Fig. 3 Cu-K edge EXAFS spectra of Cu-Mn mixed oxides.

Fig. 4 Mn-K edge XANES spectra of Cu-Mn mixed oxides. (a) Normalized spectra, (b) The first derivatives of the normalized spectra.

Fig. 5 Cu-K edge XANES spectra of Cu-Mn mixed oxides. (a) Normalized spectra, (b) The first derivatives of the normalized spectra.

Fig. 6 XPS spectra of Cu-Mn mixed oxides. (a) Cu 2p region, (b) Mn 2p region.

Fig. 7 H_2-TPR profiles for Cu-Mn mixed oxides. Catalyst weight 0.10 g; gas composition: 5%-H_2-N_2 balance; flow rate: 30 mL/min; temperature ramp: 10 K/min.

Fig. 8 Effect of temperature on CO oxidation with Cu-Mn mixed oxide. Catalyst weight: 0.050 g; CO 0.5%-O_2 5%-He balance; gas flow rate: 100 mL/min (WHSV = 120,000 mL g^{-1} h^{-1}). Cu-Mn(1-2) (△), Cu-Mn(1-1) (○), Cu-Mn(2-1) (□), CuOx (▲), and MnOx (■).

Fig. 9 Profiles for temperature programmed reduction of Cu-Mn mixed oxides with CO. Catalyst weight: 0.050 g; CO 450 ppm, He balance; gas flow rate: 500 mL/min; temperature ramp: 10 K/min. (a) Cu-Mn(1-1), (b) Cu-Mn(1-2), and (c) Cu-Mn(2-1).

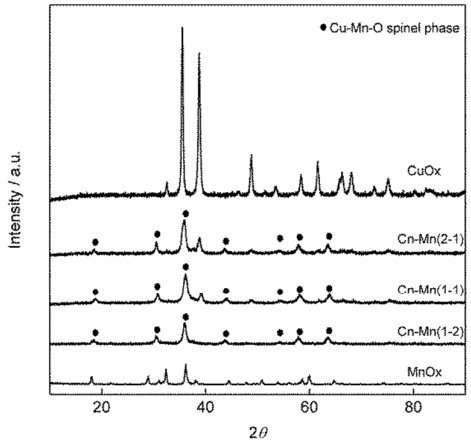

Fig. 1

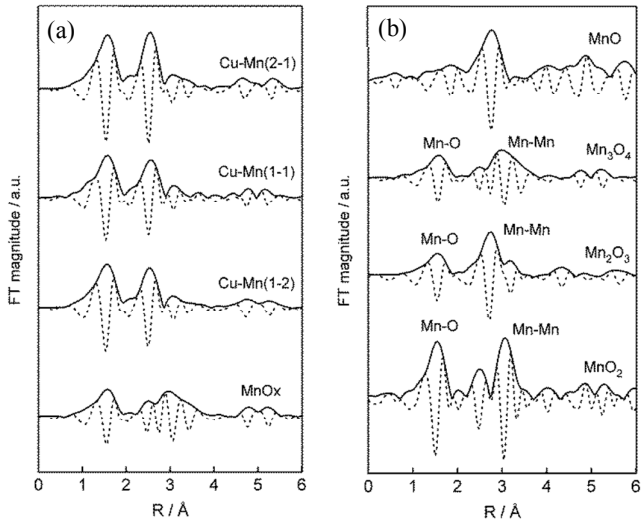

Fig. 2

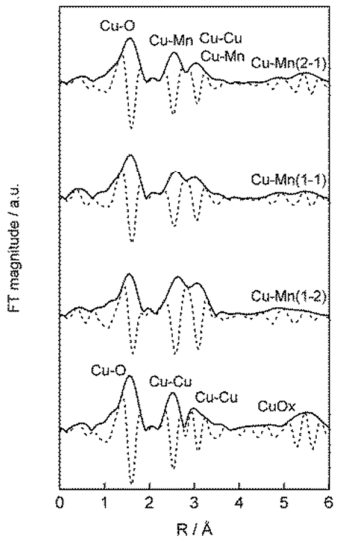

Fig. 3

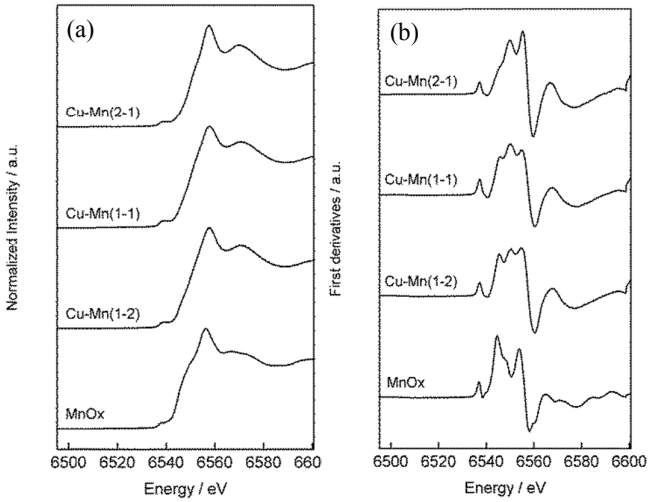

Fig. 4

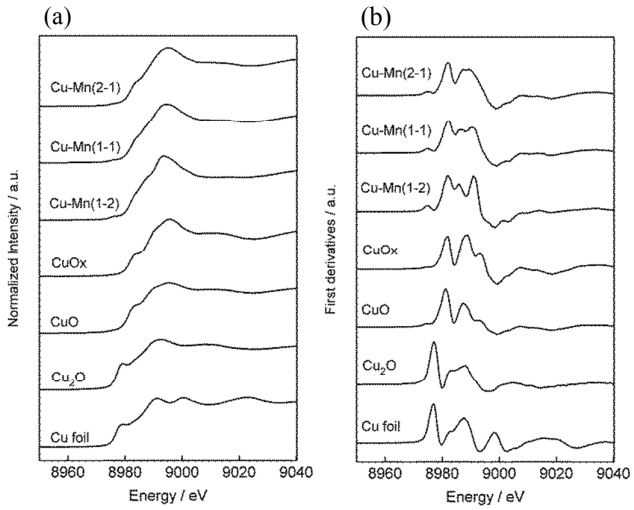

Fig. 5

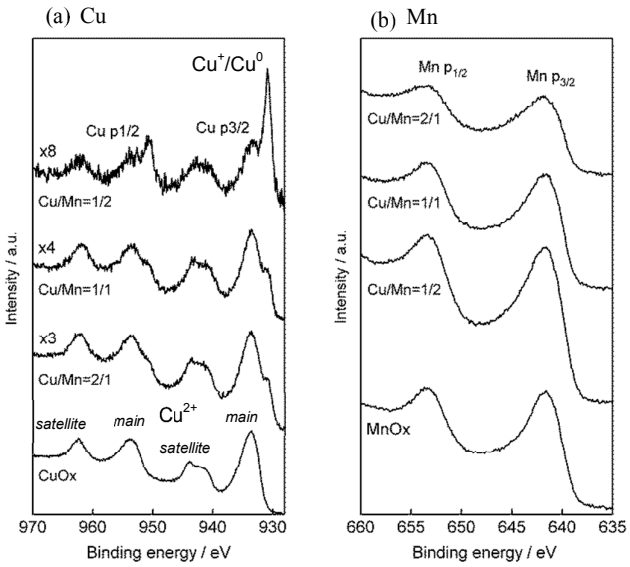

Fig. 6

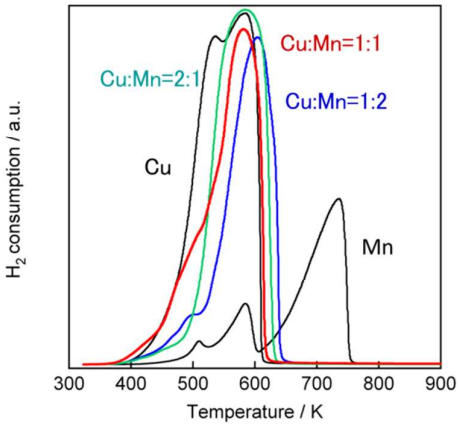

Fig. 7

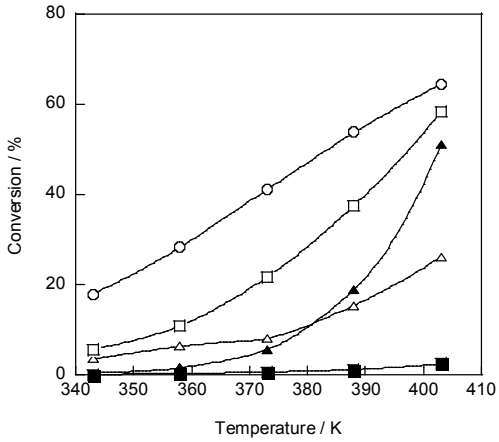

Fig. 8

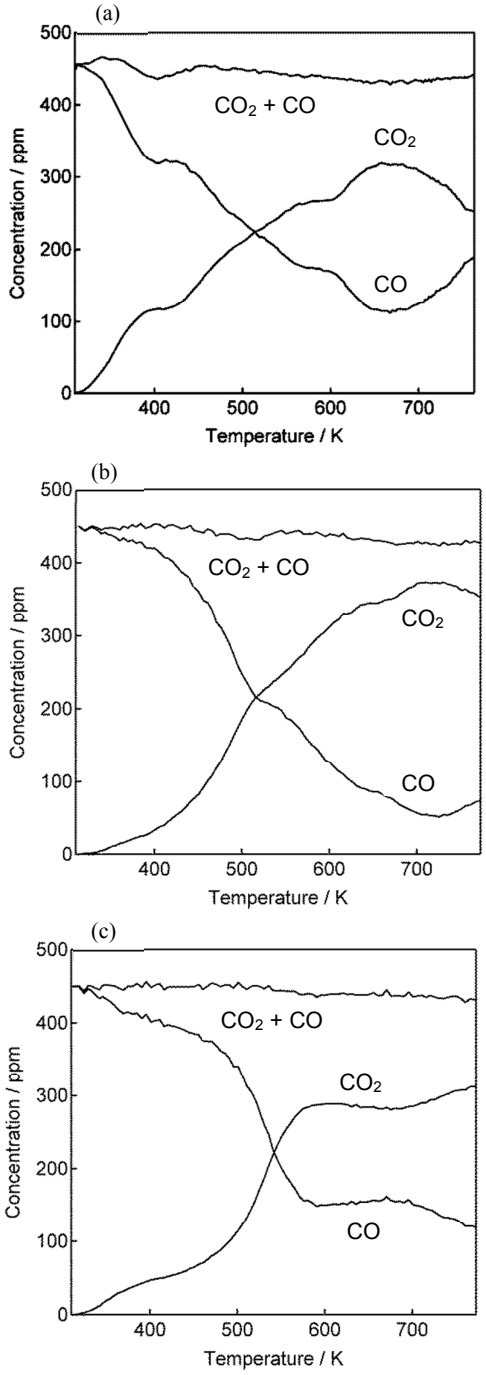

Fig. 9